J|A|C|S
JOURNAL OF THE AMERICAN CHEMICAL SOCIETY

Article

pubs.acs.org/JACS

Structural and Mechanistic Differences in Mixed-Linker Zeolitic Imidazolate Framework Synthesis by Solvent Assisted Linker Exchange and *de Novo* Routes

Krishna C. Jayachandrababu, David S. Sholl, and Sankar Nair*

School of Chemical & Biomolecular Engineering, Georgia Institute of Technology, Atlanta, Georgia 30332-0100, United States

Ⓢ *Supporting Information*

ABSTRACT: Mixed-linker zeolitic imidazolate frameworks (ZIFs) are a subclass of metal−organic frameworks (MOFs) amenable to significant property tuning by altering the functional groups on the imidazolate linkers. Solvent assisted linker exchange (SALE) and *de novo* synthesis of mixed-linker ZIFs have been demonstrated, but the differences in structural properties—most importantly the linker distributions—and synthesis mechanisms of these two different types of hybrid ZIFs are unknown. In this work, a combination of ^{1}H NMR combined rotation and multiple pulse spectroscopy (CRAMPS), water adsorption, and nitrogen measurements reveal distinct differences in linker mixing between SALE and *de novo* ZIF-8−90 hybrids. Native-fluorescence confocal microscopy is shown to provide a direct means to visualize these differences. The effects of crystal size, temperature, and SALE duration were studied in detail, and a generalizable mechanism for SALE processes in ZIFs is proposed. The SALE process is found to follow a diffusion-limited behavior leading to core−shell morphologies. Under harsher SALE conditions, deviations from diffusion-limited behavior are found due to etching and partial dissolution of the initial ZIF-8 crystals. With the selection of appropriate reaction conditions, SALE processes appear to be capable of generating controlled core−shell ZIF structures of good morphological quality that complement the well-mixed structures obtained by *de novo* methods.

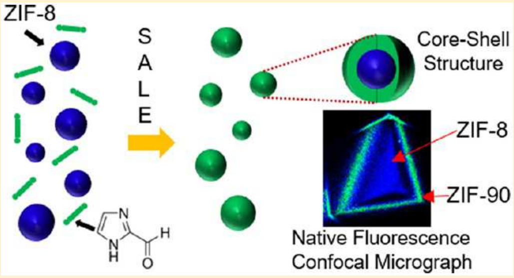

INTRODUCTION

Metal−organic frameworks (MOFs) have created great interest as materials for separation of gaseous and liquid mixtures, gas capture and storage, catalysis, drug delivery, and chemical sensing, among others.[1−5] MOFs offer a wide range of structures and pore characteristics owing to the available diversity of metal nodes and organic linker molecules.[6−8] An attractive feature of MOFs is their relative ease of synthesis, often through solvothermal routes without any templating or structure-directing agents. MOFs are also amenable to postsynthetic modification and functionalization, making it possible to obtain structures that are difficult to realize *de novo*.[9−12] In addition to MOF materials containing a single type of linker molecule, several recent studies have also shown that "mixed-linker", "hybrid", or "multivariate" MOFs can be synthesized via one-pot synthesis routes.[2,13−16] Zeolitic imidazolate frameworks (ZIFs) are a widely studied subclass of MOFs that have particularly attractive characteristics for chemical separations.[17−22] Several hybrid ZIFs have been synthesized with combinations of different imidazolate linkers.[23−26] In cases where one can synthesize a series of hybrid ZIFs with linker compositions intermediate between two single-linker ZIFs, it has been shown that continuous tuning of functional properties such as adsorption and diffusion is possible.[23−25,27−29] It is also possible to postsynthetically replace linker molecules and incorporate other linkers into MOFs using solvent assisted linker exchange (SALE) or solvent assisted linker incorporation (SALI) routes.[30−36] SALE has been demonstrated in several MOF systems such as the MIL-series, UiO-series, and PPF-series (all with carboxylate-based linkers), as well as the ZIF and CdIF series (imidazole-based linkers).[30]

Although a number of interesting demonstrations of SALE and *de novo* mixed-linker MOF synthesis have been reported, there is no systematic understanding of structural and mechanistic differences between the two techniques that lead to important functional differences between the two types of materials. The differences in linker distribution between SALE and de novo mixed-linker MOFs could create substantial differences in their properties, but these differences are not well characterized. Furthermore, while *de novo* synthesis can be understood by a relatively straightforward mechanism involving incorporation of different types of linkers during crystallization, the SALE mechanism has not been investigated in detail, and there is no overarching mechanism proposed that can explain how different MOF materials respond to SALE. Key aspects of SALE, including the role of solvents and the mechanisms of exchange (single-crystal to single-crystal versus dissolution-and-recrystallization), are not well understood.[30] MOFs with the same or similar linkers but different metal centers can display extremely different responses to SALE. For example, MIL-53

Received: February 16, 2017
Published: April 7, 2017

DOI: 10.1021/jacs.7b01660
J. Am. Chem. Soc. 2017, 139, 5906−5915

and MIL-68 MOFs (containing aluminum/indium centers) can be easily modified via postsynthetic exchange, whereas MIL-101 (chromium centers) is inert to exchange.[12]

In the context of the above issues, there are two main elements of this work. First, we investigate how mixed-linker/hybrid ZIF materials synthesized through both the SALE route and *de novo* routes have considerably different linker distributions and properties even when their bulk compositions are the same. This study focuses on the ZIF-8−90 series of mixed-linker ZIFs, which is particularly interesting because ZIF-8 and ZIF-90 are isoreticular (cubic SOD topology) and the hybrids are known to maintain the same topology throughout the entire mixed-linker composition range.[23] We synthesize a family of ZIF-8−90 hybrids using both the above routes and characterize their differences at multiple length scales. We use their water and nitrogen adsorption behavior to understand differences in their macroscopic properties. We study their microscopic structural heterogeneity using 2D ^{1}H NMR measurements and present a technique to compare the degree of linker mixing between different types of hybrid ZIFs or MOFs (e.g., synthesized by SALE versus *de novo*). Second, we conduct a detailed mechanistic study of ZIF-8 → ZIF-90 SALE and obtain insights into the propagation of SALE reactions by controlling the crystal size and temperature and using solution-NMR to monitor the process as a function of time. We also show that fluorescent confocal microscopy can be very useful to directly monitor the linker exchange process and the distribution of linkers over entire crystals. We then combine the detailed information obtained to propose a mechanism for the SALE process in ZIFs.

■ EXPERIMENTAL METHODS

Materials. Zinc nitrate hexahydrate (Alfa Aesar), 2-methylimidazole (2-MeIm) and 1-methylimidazole (1-MeIm) (Sigma-Aldrich), imidazole-2-carboxaldehyde (OHC-Im), sodium formate (Alfa Aesar), and methanol (EMD) were used as received.

Synthesis of ZIF-8 Nanocrystals. ZIF-8 nanocrystals were synthesized via the procedure given by Cravillon et al.[37] Specifically, 2.933 g of $Zn(NO_3)_2·6H_2O$ was dissolved in 200 mL of methanol. Separately, 6.489 g of 2-MeIm was dissolved in 200 mL of methanol. The first solution was rapidly poured into the second solution while stirring with a magnetic bar. The mixture turned turbid slowly, and the stirring was stopped after 1 h. The nanocrystals were collected by centrifugation at 8500 rpm for 20 min, washed with methanol, and finally redispersed in methanol to form a suspension. Small portions of this suspension were dried and degassed separately for characterization purposes. The reported yield for this procedure is 50% (Zn basis). Particle size analysis of over 200 particles using SEM showed a unimodal distribution centered at 36.5 nm with a standard deviation of 4 nm.

Synthesis of ZIF-8 Microcrystals. ZIF-8 microcrystals were synthesized by modifying the procedure given by Zhang et al.[38] Here, 0.734 g of $Zn(NO_3)_2·6H_2O$ was dissolved in 50 mL of methanol, whereas 0.810 g of 2-MeIm and 0.810 g of 1-MeIm were dissolved in another 50 mL of methanol. The first solution was poured into the second solution while stirring with a magnetic bar. Stirring was stopped upon mixing of both solutions, and the stir bar was removed. The mixture was sealed with Parafilm and left undisturbed overnight. Crystals were collected, washed with fresh methanol three times, air-dried at 60 °C, and then degassed at 180 °C for 24 h in a vacuum oven. This synthesis produced 80 mg of crystals with approximately 15% yield (Zn basis). Particle size analysis of over 400 particles using SEM showed a bimodal distribution with modes at 1.1 and 2.4 μm.

Synthesis of ZIF-8 Macrocrystals (>100 μm Size). Large ZIF-8 macrocrystals were synthesized by using the following procedure. $Zn(NO_3)_2·6H_2O$ (1.764 g) was dissolved in 20 mL of methanol. 2-MeIm (0.973 g) and sodium formate (0.404 g) were dissolved in 20 mL of methanol. The two solutions were mixed and transferred into a Teflon liner. A glass slide was also inserted into the liner. The liner was then sealed inside a Parr stainless-steel reactor and incubated in an oven at 90 °C for 6 h. The reactor was cooled slowly to room temperature under ambient conditions. Crystals were collected from the sides of the glass slide and washed with methanol three times. This synthesis produced 200 mg of crystals with approximately 15% yield (Zn basis). Particle size analysis of 20 particles using SEM showed that the crystal sizes were centered around 130 μm with a standard deviation of 32 μm.

***De Novo* Synthesis of Mixed-Linker ZIF-8−90 Crystals.** Mixed-linker ZIF-8_x−90_{100-x} crystals (where x and $100-x$ are the percentages of ZIF-8 and ZIF-90 linkers in the crystal) were synthesized by the non-solvent-induced crystallization (NSIC) procedure of Thompson et al.[23,38] ZIF-8_{50}−90_{50} was synthesized as follows: 2.974 g of $ZnNO_3·6H_2O$ was dissolved in 100 mL of methanol, and 2.874 g of 2-MeIm, 0.480 g of OHC-Im, and 2.72 g of sodium formate were dissolved in 100 mL of methanol by heating to 60 °C. After cooling the linker solution to room temperature, the zinc salt solution was poured into it rapidly with stirring. The stirring was stopped after 1 h, and crystals were recovered by centrifugation and washed three times with fresh methanol. The crystals were then air-dried at 60 °C and degassed at 180 °C in vacuum. This synthesis produced 500 mg of crystals with approximately 20% yield (Zn basis). Particle size analysis of 100 particles using SEM showed a size distribution centered at 3 μm with a standard deviation of 1.1 μm.

***De Novo* Synthesis of Mixed-Linker ZIF-8−90 Macrocrystals (>100 μm Size).** Large mixed-linker ZIF-8_{75}−90_{25} crystals were synthesized using the following procedure: 0.595 g of $Zn(NO_3)_2·6H_2O$ was dissolved in 40 mL of methanol, and 0.571 g of 2-MeIm, 0.099 g of OHC-Im, and 0.544 g of sodium formate were dissolved in 40 mL of methanol by heating to 60 °C. This solution was allowed to cool down to room temperature. Both solutions were then mixed and sealed in a glass jar. The jar was then heated to 90 °C in an oil bath for 24 h. Crystals were collected from the side of the jar and washed with fresh methanol thrice. This synthesis produced 200 mg of crystals with approximately 40% yield (Zn basis). Particle size analysis of 100 particles using SEM showed a size distribution centered at 93 μm with a standard deviation of 43 μm.

Solvent Assisted Linker Exchange (SALE). To perform SALE on ZIF-8 nanocrystals, 0.961 g of OHC-Im was dissolved in 50 mL of methanol at 60 °C under stirring. After this solution was cooled to room temperature, 40 mL of ZIF-8 nanocrystals suspended in methanol was added. The two solutions were mixed thoroughly using low-intensity ultrasonication using a VWR ultrasonication water bath, operating at 120 W and 40 kHz. The resulting mixture was then sealed and kept in an oven at 60 or 90 °C for durations of 4−192 h. To perform SALE on ZIF-8 microcrystals and macrocrystals, 0.480 g of OHC-Im was dissolved in 40 mL of methanol by heating to 60 °C under stirring. This solution was transferred to a Teflon liner and 60 mg of ZIF-8 microcrystals were dispersed in it. The mixture was then sealed in a Parr stainless-steel reactor with a Teflon insert and kept in an oven at 60 or 90 °C for durations of 4−288 h. The crystals were then recovered by centrifugation, washed in methanol repeatedly to remove unreacted linkers, air-dried at 60 °C, and degassed at 180 °C under vacuum.

Characterization. X-ray diffraction (XRD) measurements were performed on powder samples using an X'Pert Pro PANalytical diffractometer (Cu Kα source, $\lambda = 0.1.541$ nm) over a 2θ range of 3−45°, with powder samples being dispersed on a low-background sample holder. Scanning electron microscopy (SEM) images were collected on a Hitachi SU8010 field emission microscope operating at 3 kV. Water adsorption isotherms were collected on a TA Instruments VTI vapor sorption analyzer. Nitrogen physisorption isotherms were collected at 77 K using a Microtrac Belsorp-Max analyzer. Composition analysis of the hybrid ZIFs were carried out using a Bruker Avance III 400 MHz solution-state nuclear magnetic resonance (NMR) spectrometer after dissolving the ZIF in deuterated (d_4)-acetic acid. ICP-MS analysis of the post-SALE supernatant solution was

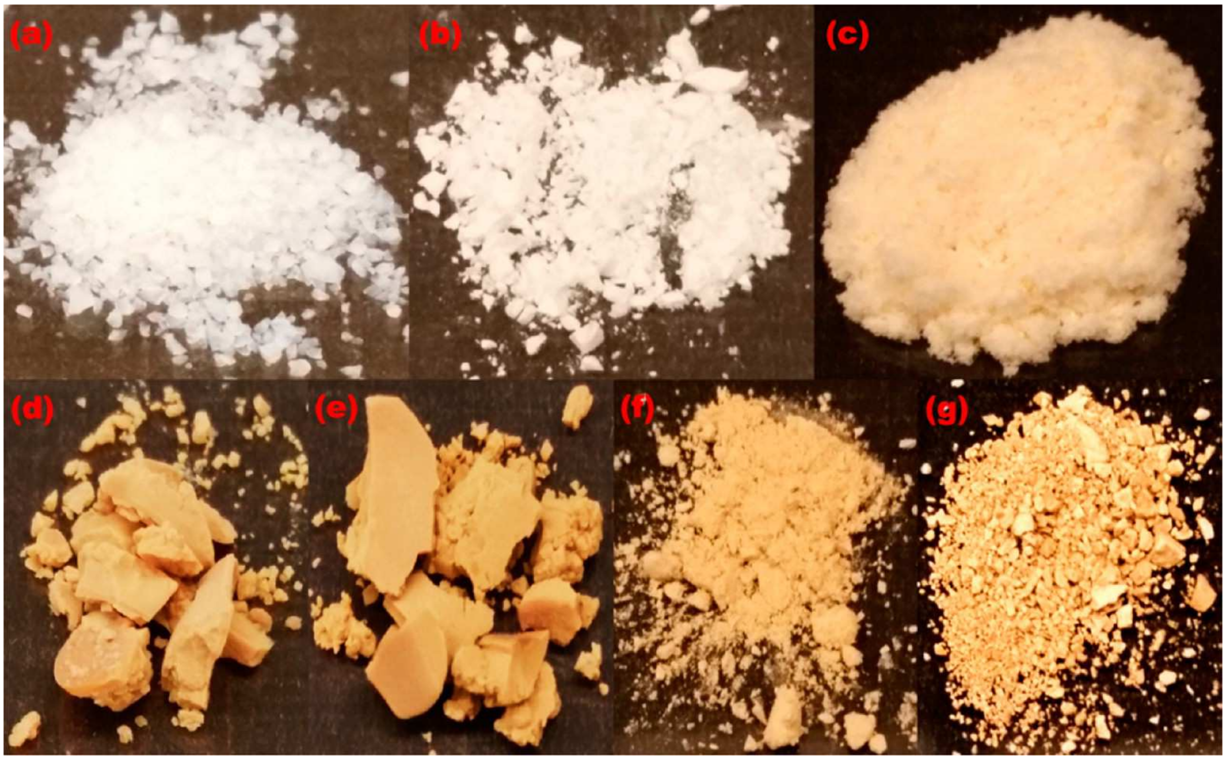

Figure 1. (a) ZIF-8 nanocrystals, (b) ZIF-8 microcrystals, (c) ZIF-8_{50}−90_{50} NSIC hybrid, (d) nano-ZIF-8−90 SALE hybrid made at 60 °C for 3 days, (e) nano-ZIF-8−90 SALE hybrid made at 90 °C for 8 h, (f) micro-ZIF-8−90 SALE hybrid made at 90 °C for 3 days, and (g) micro-ZIF-8−90 SALE hybrid made at 60 °C for 6 days. Each image occupies roughly 2.5 × 2.5 cm^2 area.

performed using a PerkinElmer NexION 300Q ICP-MS with a PerkinElmer multielement calibration standard 3 (without mercury). As described in detail by us recently,[39] spin diffusion (2D CRAMPS) data was collected using a Bruker Avance III 400 MHz solid-state NMR spectrometer with a standard broadband H/X MAS probe. About 5 mg of sample was loaded into a ZrO_2 rotor and the magic angle spinning (MAS) speed was set at 5 kHz. No recoupling was applied during the mixing time. Phase modulated Lee−Goldburg (PMLG) decoupling was used during the evolution and detection times (Bruker pulse sequence: wpmlg2d).[40,41] We used mixing times from 0.1 to 50 ms, 399.92 MHz Larmor frequency, 2.5 μs $\pi/2$ pulse width, 56.57 kHz frequency offset, 12.5 μs Lee−Goldburg 2π pulse, receiver gain of 8, 4 scans, and 512 × 128 2D points with sine apodization. Confocal microscopy was performed on a combination Zeiss LSM 780/PS.1 super-resolution microscope equipped with a standard photomultiplier tube, 32-channel spectral GaAsP detector, and a cooled GaAsP detector.

■ RESULTS AND DISCUSSION

We first performed SALE experiments on ZIF-8 nanocrystals (36 ± 4 nm average size) and microcrystals (bimodal size distribution with 1.1 ± 0.4 μm and 2.4 ± 0.3 μm populations). Figure 1 shows photographs of the different ZIF materials studied. Before SALE was initiated, both types of ZIF-8 crystals were colorless (Figures 1a,b). Upon addition of the OHC-Im (ZIF-90) linker solution to the nanocrystal ZIF-8 suspension, both types of crystals rapidly changed color to a pale brown tint (Figures 1d−g). Upon visual inspection, the color of the crystals after short (~4 h) and long (up to 6 days) SALE durations were virtually indistinguishable. In contrast, crystals of hybrid ZIF-8−90 materials synthesized via the NSIC route (Figure 1c) possess an off-white shade, which becomes darker with increasing amount of the ZIF-90 linker in the crystal. Neat 2-MeIm crystals are colorless, whereas OHC-Im crystals are pale yellowish-brown. The appearance of color in ZIF-8 crystals undergoing SALE with ZIF-90 linkers suggests that the surface 2-MeIm linkers on ZIF-8 crystals have been exchanged with OHC-Im. The dissimilar visual appearance of NSIC and SALE hybrid ZIF-8−90 materials, even after long exchange times, points to significant differences in microscopic linker mixing levels in the two types of materials.

To study the linker distribution, two SALE-processed samples (one nanocrystalline and one microcrystalline) were prepared with the same overall composition of ZIF-8_{50}−90_{50} (determined by ^{1}H-solution NMR). An NSIC ZIF-8_{50}−90_{50} hybrid was also synthesized for comparison. Figure 2 shows XRD patterns of ZIF-8, ZIF-90, the NSIC hybrid, and the SALE hybrids. It is clear that regardless of the linker composition or synthesis route, all members of the ZIF-8−90 family maintain the same SOD topology with near-identical peak positions and intensities. However, subtle changes in the low-angle peak positions of the parent ZIFs, SALE hybrids, and the NSIC hybrid can be observed (Figure S1, Supporting Information) and are due to the changes in unit cell parameters. Recently, high-resolution powder X-ray diffraction (HR-PXRD) and density functional theory (DFT) calculations have been used to study structure−property relationships of mixed-linker UiO-66 materials made by direct synthesis and postsynthetic exchange.[42] This method facilitates accurate measurement of unit-cell parameters with varying linker fractions, but information about linker segregation/mixing is not obtained.

Solid-state NMR spectroscopy has been used recently to study linker mixing patterns in mixed-linker MOF systems.[43,44] For example, we used a combination of ^{1}H-CRAMPS NMR and computational generation of candidate structures to probe the degree of linker mixing in *de novo* ZIF-8−90 NSIC hybrids.[39] This technique is based upon measuring spin

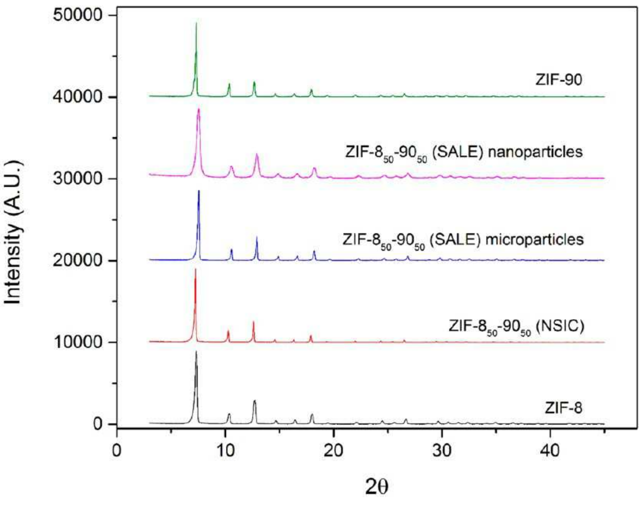

Figure 2. Powder XRD patterns of ZIF-8, ZIF-90, NSIC hybrid, and SALE hybrids. The patterns are stacked vertically for convenience of display.

exchange between protons on the linker functional groups ($-CH_3$ and $-CHO$ in ZIF-8 and ZIF-90, respectively). Spin exchange in ZIF crystals is governed by dipolar coupling, whose strength is a strong function of the distance between the nuclei involved. Thus, the rate of spin transfer is dependent upon the degree to which the two linkers are mixed or interspersed in the crystal. Experimentally, we measure the magnetization ratios of the source and sink protons participating in spin transfer (in this case, the 2-MeIm methyl protons and the OHC-Im aldehyde protons, respectively). By monitoring the degree of spin exchange as a function of mixing time, and comparing to kinetic model predictions of spin exchange in computationally generated candidate structures, we showed that the linkers in *de novo* ZIF-8−90 hybrids are mixed at a unit cell level and can be characterized using the Warren−Cowley short-range order (SRO) parameter.[39,45]

Figure 3 shows the differences in spin exchange profiles between the SALE and *de novo* (NSIC) hybrids. For qualitative understanding of spin exchange processes in materials, one can use a widely applied model that approximates the microscopic spin exchange between discrete, homogeneously distributed nuclei as a Fickian "spin diffusion" process.[46−49] Accordingly, the intensity ratio of the sink and source signals is plotted as a function of the square root of mixing time (in $ms^{0.5}$) in Figure 3. The key aspects to note are the spin diffusion behavior at short mixing times (<1 $ms^{0.5}$) and at long mixing times (>4 $ms^{0.5}$). The NSIC hybrid shows a linear increase in spin transfer at short mixing times, consistent with Fickian behavior expected when the linkers are well-mixed. As shown in our previous work,[43] the effective Fickian "spin diffusivity" in ZIF-8 and ZIF-90 is ∼0.2 $nm^2 \cdot ms^{-1}$. This leads to a mixing length scale of ∼2 nm for the NSIC hybrids based upon the slope of the linear region. Thus, it is clear that the linkers are mixed on a unit-cell level. Finer details of the linker distribution were previously characterized in terms of the SRO parameter using a full kinetic model of the spin exchange between the discrete nuclei.[43] On the other hand, the SALE hybrids exhibit a significant lag period before appreciable spin exchange is observed, as well as a slower spin transfer rate than the NSIC hybrids. This suggests that the two spin domains (the methyl group and aldehyde group) in the SALE hybrid are more segregated than in the NSIC materials. The initial lack of spin exchange signal is due to the weak proton−proton dipolar coupling resulting from the much longer distances between 2-MeIm and OHC-Im in the SALE hybrids. In segregated structures, the only spins that can participate in spin exchange at short mixing times are those at the interfaces of the two types of domains, which represent only a small fraction of the total number of linkers in the material.

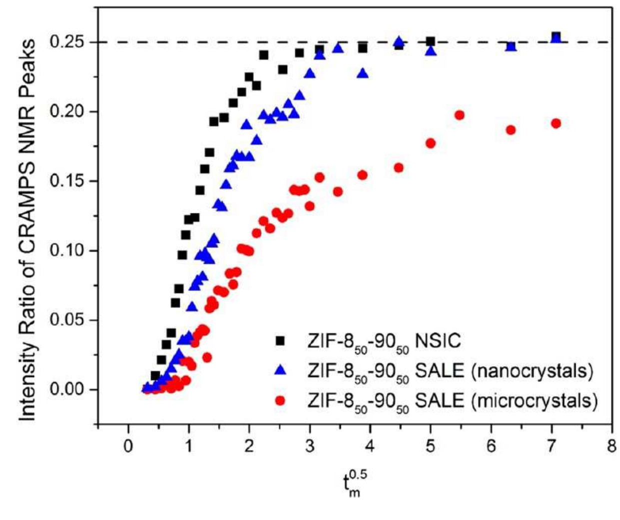

Figure 3. ^1H CRAMPS NMR peak intensity ratio plotted versus the square root of mixing time (in units of $ms^{0.5}$) for three different types of ZIF-8−90 hybrids of identical overall composition.

For the NSIC hybrid, the asymptotic value of the intensity ratio curve at long mixing times can be predicted *a priori* (as marked by the dashed line in Figure 3) based on the relative numbers of the two types of protons. The experimental data is seen to reach this asymptotic value (which is 0.25 for a ZIF-$8_{50}-90_{50}$ hybrid). In the nanocrystal SALE hybrid, spin exchange proceeds more slowly than the NSIC hybrid but reaches the asymptote at a longer mixing time. In the microcrystal SALE hybrid, the spin transfer does not reach the asymptote even at very long mixing times. The nanocrystals have a much larger surface area-to-volume ratio (about 100 times that of the microcrystals), and as a result, the interfaces between the two spin domains contribute significantly more to the signal than in the microcrystals. Overall, the spin diffusion measurements allow a way to qualitatively assess whether the linkers in a hybrid MOF/ZIF are microscopically mixed, with a resolution approaching unit cell dimensions. In particular, we find that the present SALE materials are not in fact well-mixed hybrid ZIFs but rather display considerable segregation or clustering of the linkers.

Figure 4 shows water adsorption and nitrogen physisorption isotherms for pure ZIF-8 and ZIF-90, a physical mixture of ZIF-8 and ZIF-90 crystals, and the ZIF-8−90 hybrids made by both SALE and NSIC. In Figure 4a,b, the physical mixture exhibits adsorption properties that are a simple weighted sum of the properties of ZIF-8 and ZIF-90, as expected. The NSIC hybrid ZIF-8−90 material displays distinct adsorption behavior from the "parent" ZIF-8 and ZIF-90 materials. The water adsorption isotherm shows a pore filling pressure ($P/P_0 \approx 0.7$) distinct from ZIF-90 ($P/P_0 \approx 0.55$) and ZIF-8 (which is highly hydrophobic and does not display a pore-filling pressure under the present conditions). Furthermore, the saturation loading of water in the NSIC hybrid is equivalent to that of ZIF-90 since the entire pore volume is available for adsorption. The nitrogen

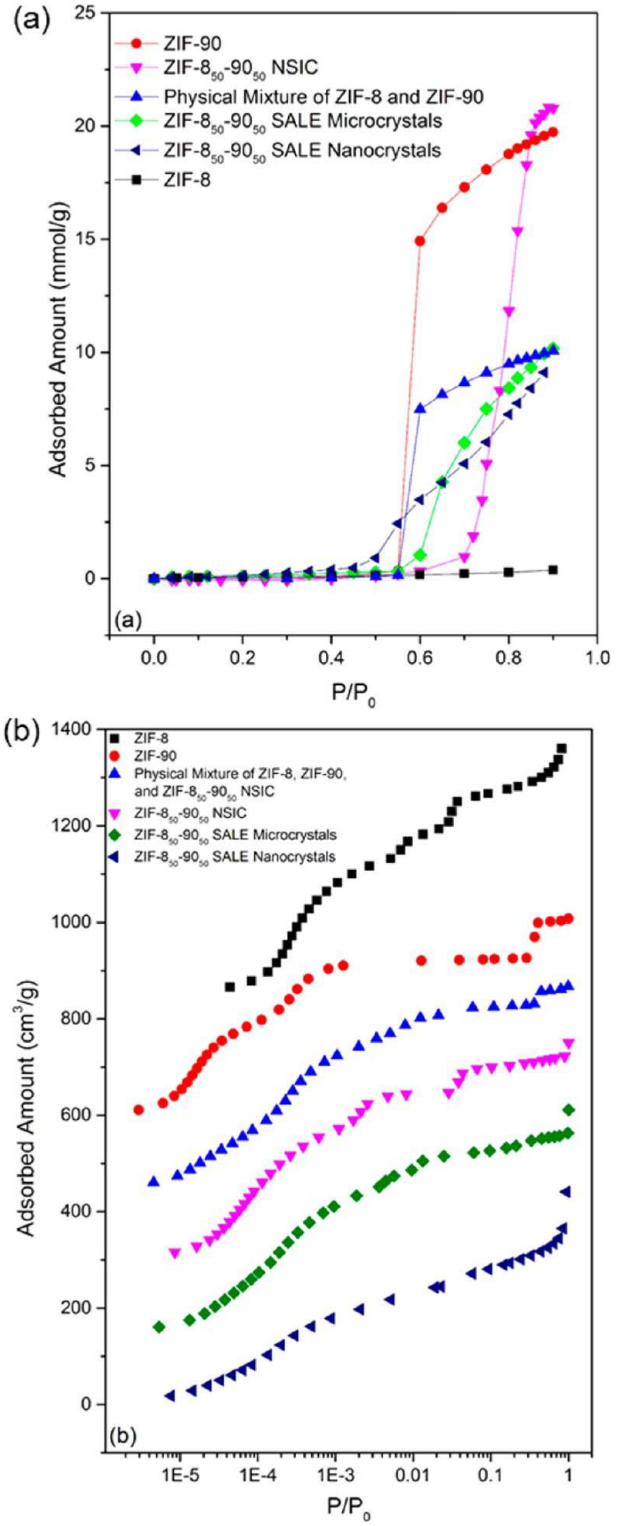

Figure 4. (a) Water adsorption isotherms and (b) nitrogen physisorption isotherms of ZIF-8, ZIF-90, physical mixture of ZIF-8/ZIF-90, NSIC hybrids, and SALE hybrids. Isotherms in panel b are offset by 150 cm^3/g for convenience of display.

physisorption isotherm also displays "gate-opening" inflections distinct from those of the parent materials. This behavior, as also observed in our earlier work, is due to the fact that the pore windows in the NSIC hybrid are lined with both types of linkers,[39] thereby conferring a distinct set of adsorption and diffusion characteristics in comparison to the parent materials.[23,24] The SALE hybrids display sharply contrasting behavior from the NSIC hybrids. The water adsorption isotherms show pore filling pressures ($P/P_0 \approx 0.55{-}0.6$) close to that of ZIF-90 but a much lower saturation loading than ZIF-90. This behavior clearly indicates the presence of distinct ZIF-90-rich domains (which allow pore-filling water uptake) and ZIF-8-rich domains (which remain inaccessible to water). The nitrogen physisorption isotherms of the SALE hybrids resemble that of the physical mixture of ZIF-8 and ZIF-90, further indicating the presence of ZIF-8-rich and ZIF-90-rich domains. The quite different functional properties of the hybrid ZIF materials synthesized by NSIC and SALE routes further support our hypothesis that they have drastically different degrees of linker mixing. The relatively minor differences between the isotherms of the SALE nanocrystals and microcrystals are caused by particle size and packing effects. The nanocrystal sample contains a greater number of mesopores (formed due to close nanoparticle packing), resulting in greater capillary condensation of adsorbates at higher pressures. The structural transition of ZIF-8 induced by nitrogen adsorption also occurs at a higher pressure for nanocrystals as compared to microcrystals.[38] All the materials shown in Figure 4 have comparable textural properties such as the BET surface area. These values are obtained as ZIF-8 (1341 m^2/g), ZIF-90 (1100 m^2/g), physical mixture (1271 m^2/g), NSIC ZIF-8$_{50}$−90$_{50}$ (1478 m^2/g), SALE nanocrystal ZIF-8$_{50}$−90$_{50}$ (1471 m^2/g), and SALE microcrystal ZIF-8$_{50}$−90$_{50}$ (1494 m^2/g).

While the foregoing discussion gives substantive information about linker distributions in the hybrid ZIF crystals, so far no technique has been reported for direct visualization of linker distribution. To this end, we hypothesized that the native fluorescence of the imidazolate linkers (attributed to $\pi^*{-}\pi^*$ transitions[50,51]) could be used to obtain such information. In particular, ZIF-8 crystals emit blue light (460 nm) and ZIF-90 crystals emit green light (505 nm) when excited by a 405 nm wavelength laser. The intensity of emission by ZIF-90 is considerably stronger than that of ZIF-8. Combining this fluorescence behavior with confocal microscopy, we can obtain information on linker distribution throughout the bulk of *de novo* and SALE hybrid macrocrystals (>100 μm size). Thus, a 3D mapping of the linker distribution near the surface as well as the interior of the crystals can be obtained using true-color fluorescence imaging, without the necessity of labeling with dye molecules. Figure 5a,b shows cross sections of ZIF-8 and ZIF-90 crystals undergoing fluorescent emission. The insets show the orientations of these crystals relative to the objective lens of the microscope. Figure 5c shows emission from two crystals of a ZIF-8$_{75}$−90$_{25}$ hybrid made via *de novo* synthesis. The composition was deliberately skewed toward a ZIF-8-rich hybrid to compensate for the higher intensity of fluorescence from ZIF-90 linkers. This material emits both blue and green light, and the combined effect produces a cyan color. The presence of ZIF-8 and ZIF-90 throughout the entire crystal can be seen by filtering the images to show the blue and green emissions separately (inset of Figure 5c). There is uniformly distributed emission at both wavelengths throughout the cross-section. The Supporting Information contains movies of the observed emission from entire crystals, obtained by combining the scans from multiple focal planes (cross sections). Figures S2−S5 (Supporting Information) depict the crystal orientations corresponding to each movie. The blue and green emissions are uniformly distributed throughout the crystals (videos A−E),

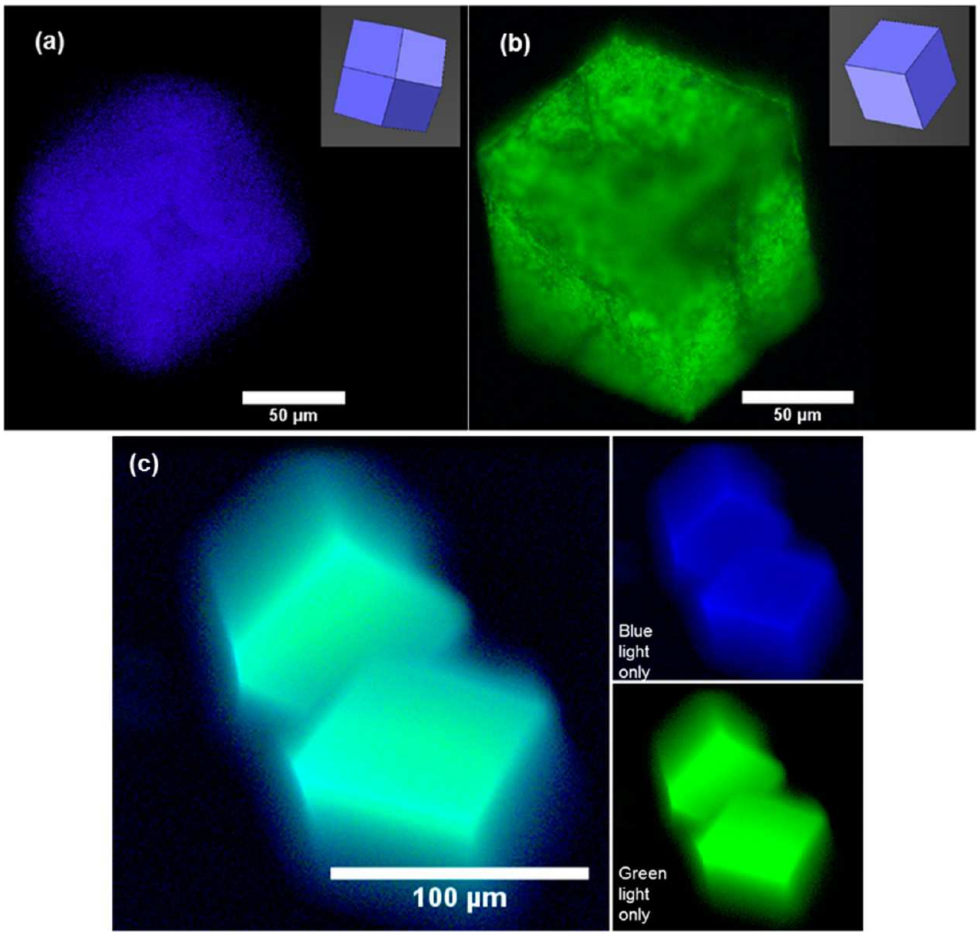

Figure 5. Fluorescent confocal images of (a) ZIF-8 crystal, (b) ZIF-90 crystal with relative crystal orientations in the inset, and (c) a *de novo* ZIF-8_{75}−90_{25} hybrid (with blue and green emissions shown separately in the inset). Blue and green emissions correspond to fluorescence from ZIF-8 linkers (2-MeIM) and ZIF-90 linkers (OHC-Im) respectively.

which is characteristic of a hybrid ZIF with the linkers being well-mixed.

On the other hand, Figure 6a−d shows fluorescence from a ZIF-8_{90}−90_{10} SALE hybrid crystal at four different focal planes (cross sections), and the Supporting Information (videos F−H) shows movies constructed from confocal imaging of several different SALE hybrid crystals. SALE on these macrocrystals proceeds very slowly due to diffusion limitations, and even after prolonged exchange periods (>48 h) only 10% of 2-MeIm linkers are replaced with OHC-Im linkers. Further exposure causes morphological defects in the particles (discussed in detail below). The use of smaller crystals was not feasible due to the limitations of the confocal microscope, which has a spatial resolution of ~1 μm due to the strong native fluorescence from the ZIF linkers. It is seen that the distribution of ZIF-90 linkers (green color) is limited to the outer edges of the crystals and that the interior of the crystals contain only ZIF-8 linkers (blue color). Thus, the SALE of ZIF-8 macrocrystals to ZIF-8−90 hybrid macrocrystals proceeds from the external surface and creates a core−shell type of compositional distribution. This is in agreement with the "apparent physical mixture" behavior exhibited during water and nitrogen adsorption, the slow spin exchange observed in CRAMPS NMR, and the visual appearance of SALE hybrids (brown color). The confocal microscopy results reported here are, to our knowledge, the first direct visual confirmation of linker mixing or segregation in *de novo* and SALE MOF hybrids, respectively. This core−shell type distribution is similar to the result obtained for MOF-5/IRMOF-3 core−shell architectures verified using optical microscopy.[52] But unlike the MOF-5/IRMOF-3 crystals grown using a seeding method, no new metal source is added to the solution during SALE, and therefore the mechanisms are not comparable. A ZIF-8/ZIF-67 core−shell system has also been reported in literature.[53] These crystals were also synthesized via a seed-mediated technique and hence use additional metal ions to grow the shell layer. No comparison of structure or properties with a well-mixed ZIF-8−67 hybrid was made.

We then performed a more detailed mechanistic study of the SALE process. Figure 7 shows the linker composition of (originally) ZIF-8 nanocrystals and microcrystals as a function of the SALE processing time at temperatures of 60 and 90 °C. During each experiment, crystal samples were drawn from the SALE reactor at different times ranging from 4 h to 8 days, washed, dried, and activated. The sample was then dissolved in deuterium-substituted d_4-acetic acid, and its composition was analyzed by solution ^{1}H NMR. For both microcrystals and nanocrystals, higher temperature promotes the rate of SALE, reflecting the activated nature of the overall process. Figure 7 is plotted with the square root of time on the x-axis. At 60 °C, the nanocrystals exhibit a linear increase in OHC-Im (ZIF-90 linker) incorporation versus $t^{1/2}$ for most the SALE processing time, indicating a diffusion-limited process. A similar behavior is seen for the nanocrystals at 90 °C, except that the SALE rate is

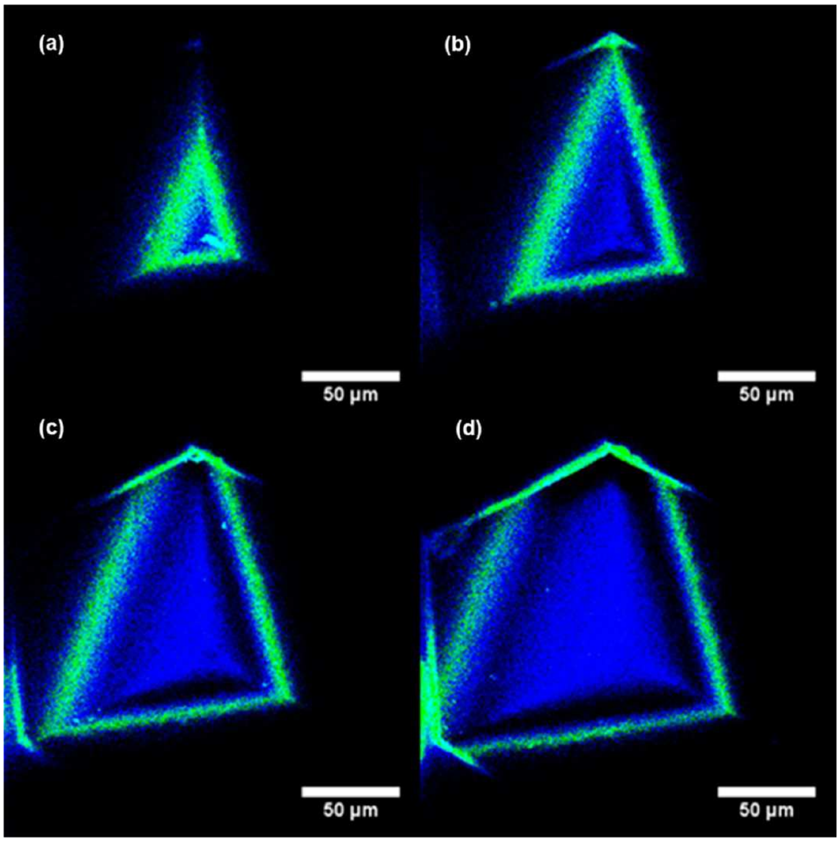

Figure 6. (a−d) Fluorescent confocal images of a SALE ZIF-8_{90}−90_{10} hybrid material at multiple focal planes moving progressively deeper into the bulk of the crystal. Blue and green emissions correspond to fluorescence from ZIF-8 linkers (2-MeIM) and ZIF-90 linkers (OHC-Im), respectively.

considerably faster (presumably due to the increased diffusivity of the linkers). The ZIF-90 linker fraction in the nanocrystals also saturates at about 90%, that is, pure ZIF-90 nanocrystals are not obtained even though a large excess (2-MeIm/OHC-Im ≈ 1:50) of ZIF-90 linkers is available in the reactor. We propose that initial exchange begins at the external surface of the nanocrystals and proceeds into the crystal but quickly becomes diffusion-limited since additional linker exchange would require the diffusion of OHC-Im linkers into the ZIF pores and the counter-diffusion of displaced 2-MeIm linkers out of the pores. The linker fraction of ZIF-90 in the crystals also saturates around 90% for SALE at both 60 and 90 °C suggesting that the exchange process has reached equilibrium. Figure 8a−c shows representative SEM images of the ZIF-8 nanocrystals before and after SALE at 60 and 90 °C, wherein it is apparent that no significant changes in crystal morphology or size distribution have occurred. Figure 7 also reveals a strong crystal size effect consistent with diffusion-limited processes. SALE on ZIF-8 microcrystals at 60 °C proceeds at a slower rate than that on nanocrystals at the same temperature and OHC-Im linker concentration in the solution. The microcrystals at 90 °C also show a linear behavior similar to the nanocrystals at shorter SALE times (up to $t^{1/2} \approx 5$). However, they subsequently show a sudden increase in linker exchange. We verified this behavior to be reproducible by performing the experiments three times for each case to estimate the error bars in Figure 7. This observation indicates that additional phenomena must be considered to provide a complete mechanistic description of SALE in these crystals.

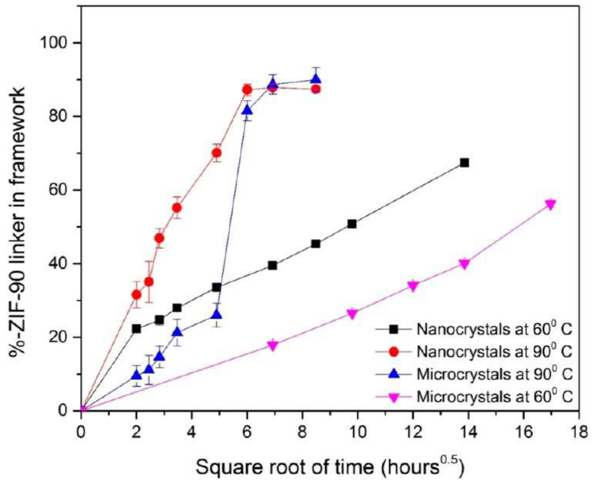

Figure 7. Composition of ZIF-8−90 SALE hybrids versus square root of time for two crystal size ranges at two temperatures. The lines joining the data points are only to guide the eye.

SEM images of the microcrystals (Figure 8d−f) do not indicate significant changes in crystal size distribution. However, Figure 8f indicates the formation of defects on the crystal surfaces at higher SALE temperatures and times (90 °C for 4 days). This is further highlighted in Figure 9a, wherein a significant fraction of crystals show surface etching or pitting and some crystals have been "hollowed out" by partial dissolution. To verify this behavior, we also performed SALE at a higher temperature of 120 °C and observed even greater etching and partial dissolution of the microcrystals (Figure 9b). This loss of ZIF-8 linkers from the solid phase partially explains

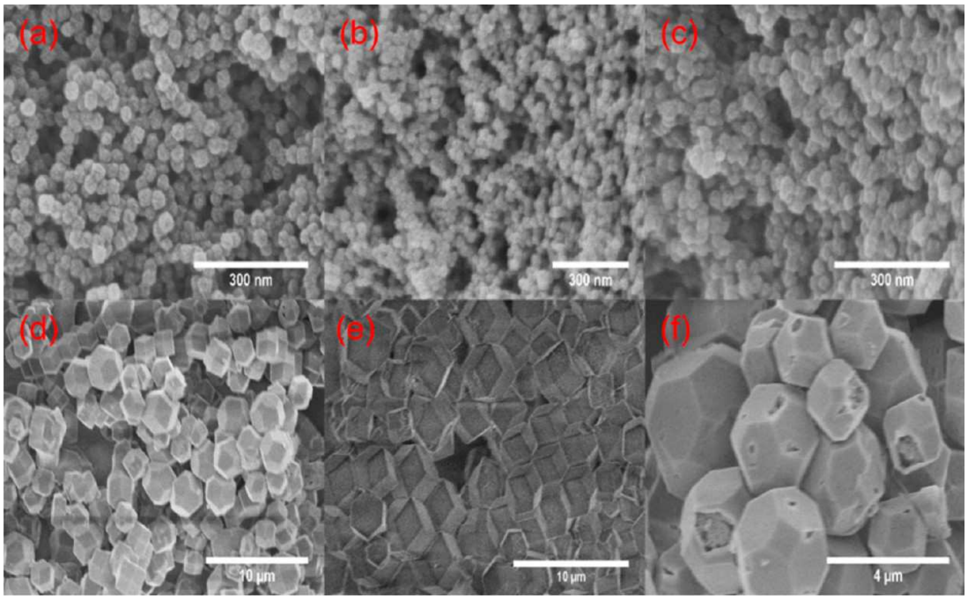

Figure 8. (a) ZIF-8 nanocrystals before SALE, (b) ZIF-8−90 nanocrystals after SALE at 60 °C for 3 days, (c) ZIF-8−90 nanocrystals after SALE at 90 °C for 8 h, (d) ZIF-8 microcrystals before SALE, (e) ZIF-8−90 microcrystals after SALE at 60 °C for 12 days, and (f) ZIF-8−90 microcrystals after SALE at 90 °C for 36 h.

the deviation from diffusion-limited exchange (i.e., a rapid increase in the ZIF-90 linker fraction) observed in Figure 7 for the microcrystals undergoing SALE at higher temperatures and times (90 °C for 4 days). Additionally, etching or partial dissolution of the microcrystals introduces both Zn^{2+} ions and ZIF-8 linkers into the initial SALE solution, which only contained ZIF-90 linkers. This solution may be capable of forming additional mixed-linker ZIF-8−90 crystals with ZIF-90 as the majority constituent owing to its excess in the solution. Finally, one must also consider the possibility that pure ZIF-90 crystals may nucleate and grow in the solution by using the Zn^{2+} ions released during etching of the ZIF-8 crystals. Both these possible mechanisms could play a role in the observed deviation from diffusion-limited behavior at harsher SALE conditions.

To investigate these issues, we first performed a control experiment in which the solution was maintained at the same conditions (temperature, time) as in the SALE process but with ZIF-8 crystals absent. In this experiment, the solution also contained zinc nitrate (with Zn/OHC-Im molar ratio of 1:4), which is a significantly higher Zn^{2+} concentration than would

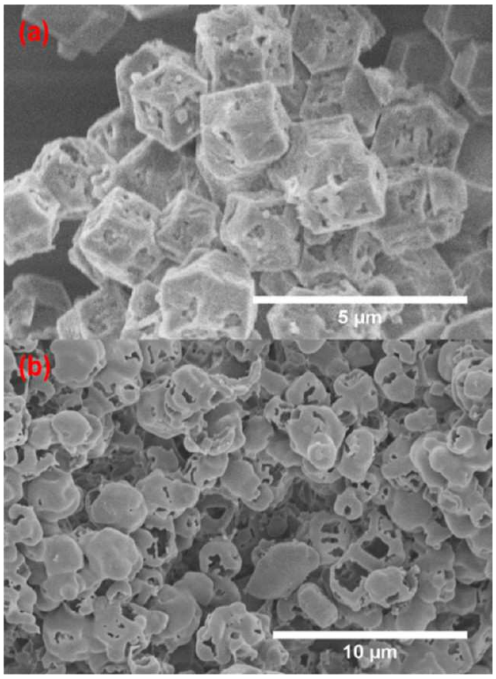

Figure 9. SEM images depicting crystal pitting and etching observed during SALE in ZIF-8 microcrystals at (a) 90 °C for 4 days and (b) 120 °C for 2 days.

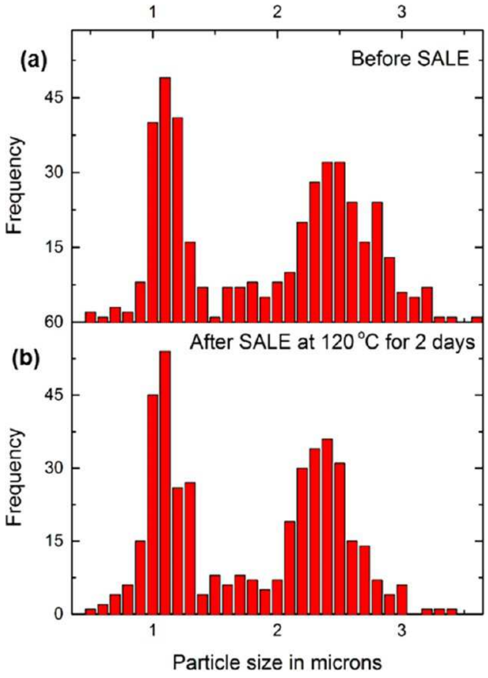

Figure 10. Size distribution of ZIF-8 microcrystals: (a) before SALE and (b) after SALE at 120 °C for 2 days.

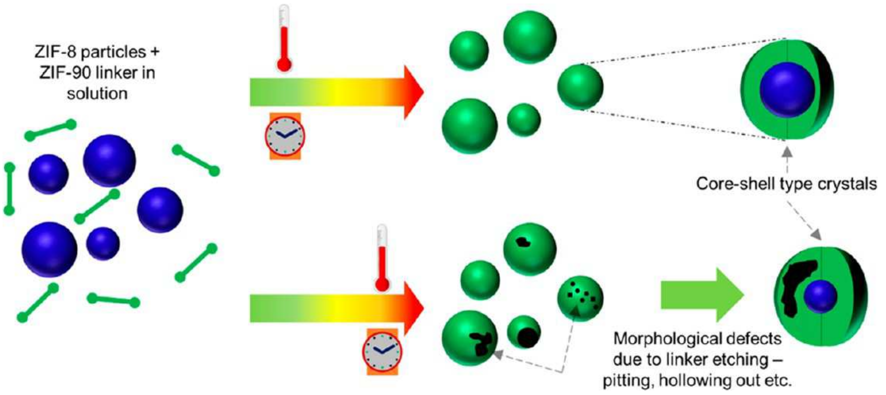

Figure 11. Schematic mechanism of ZIF-8 → ZIF-90 solvent assisted linker exchange (SALE).

be obtained if all the ZIF-8 microcrystals dissolved and released Zn^{2+} ions during SALE (~1:20). No ZIF-90 crystals were formed in this experiment, and so we can rule out the possibility of formation of pure ZIF-90 crystals during SALE. This is also in good agreement with our observation that ZIF-90 synthesis is not facile when using methanol as the synthesis medium and that all reported ZIF-90 synthesis procedures involve DMF, water, or a mixture of DMF and methanol.[54−57] However, in previous work we have crystallized mixed-linker ZIF-8−90 crystals at 90 °C by heating a solution containing only 2-MeIm, OHC-Im, and zinc nitrate in methanol.[24] In that synthesis, the Zn^{2+} concentration was 50 $mmol \cdot L^{-1}$, and the Zn/2-MeIm/OHC-Im ratio in the solution was 1:3:1. If all the ZIF-8 crystals in the present SALE experiments were to dissolve, the Zn^{2+} concentration would be 6.2 $mmol \cdot L^{-1}$ and the Zn/2-MeIm/OHC-Im ratio in solution would be roughly 1:2:20. We analyzed three supernatant solutions after SALE reactions at different temperatures and durations (13 days at 60 °C, 7 days at 90 °C, and 2 days at 120 °C) using ICP-MS. The concentrations of Zn^{2+} in these solutions were found to be in the range of only 40−130 ppm. We prepared solutions with similar concentrations of Zn^{2+} and 2-MeIm/OHC-Im ratio of 1:10. These solutions were heated to 60, 90, and 120 °C in sealed reactors. No mixed-linker ZIF-8−90 crystals were found under these conditions. Hence, in addition to ruling out ZIF-90 formation, we can also exclude mixed-linker ZIF-8−90 formation during SALE even when the original ZIF-8 crystals undergo morphological transformation by linker etching. Figure 10 shows crystal size distributions (obtained from multiple SEM images) before and after SALE at 120 °C for 2 days. The distribution is virtually unchanged after SALE, further supporting the absence of new mixed-linker ZIF-8−90 crystals forming from the solution.

■ CONCLUSIONS

We synthesized a family of mixed-linker ZIF-8−90 materials via solvent assisted linker exchange (SALE) and non-solvent-induced crystallization methods. Using ^1H-CRAMPS NMR, we demonstrated a simple way to distinguish SALE and *de novo* mixed-linker materials at a unit-cell level. The effect of linker mixing on functional properties is elucidated using water adsorption and nitrogen physisorption. We have demonstrated that these two synthesis routes can lead to hybrid ZIFs with the same overall composition but drastically different properties attributed to the difference in linker mixing achieved via these two routes. Figure 11 shows a schematic summary of the SALE mechanism in ZIF-8−90 materials, based upon all the findings of this work. This mechanism may also hold a more general validity for other ZIF systems in which diffusion of bulky imidazolate linkers through small or medium-sized pores (4−6 Å) of the ZIF framework can be expected to limit the SALE rate. Regardless of the crystal size regime (nano/micro/macro), the initial mechanism for linker exchange in such systems is seen to be a diffusion-limited process resulting in core−shell crystals. In the case of macrocrystals, these core−shell structures could be directly imaged for the first time with fluorescence confocal microscopy. In the case of nanocrystals, diffusive processes appear to be fast enough to complete the linker exchange and reach equilibrium before other processes such as crystal etching and dissolution can exert significant effects. In the case of micro- or macrocrystals, the diffusion-limited exchange is much slower and other processes become significant at extended SALE durations. The crystals undergo etching and partial dissolution, releasing significant amounts of Zn^{2+} ions and ZIF-8 linkers into the solution and leading to morphological defects such as pits and holes in the SALE-treated crystals. However, control experiments show that neither new crystals of pure ZIF-90 nor mixed-linker ZIF-8−90 are formed in the solution, When synthesizing hybrid ZIFs via SALE, care must be taken to ensure that the processing conditions do not cause damage to the ZIF material. Both the SALE and *de novo* techniques are very useful for synthesizing MOFs with controlled compositions and functionality. Our findings clearly indicate that the products of SALE and *de novo* processes for hybrid ZIF materials can be significantly different, and hence the characterization of linker mixing is of utmost importance when dealing with these materials. Furthermore, the results of SALE on different classes of MOFs will depend on factors such as particle size, linker solubility, pore size, and SALE conditions. These effects can be now analyzed and inferred from the mechanistic basis reported here, and the resulting morphologies can be different for different classes of MOFs. For example, if the MOF pore size is significantly larger than the linker size, then SALE may not be diffusion-limited and would result in a more well-mixed linker distribution.

■ ASSOCIATED CONTENT

Ⓢ Supporting Information

The Supporting Information is available free of charge on the ACS Publications website at DOI: 10.1021/jacs.7b01660.

X-ray diffraction patterns of pure and mixed-linker ZIFs and movies of multiple-focal-plane fluorescent confocal microscopy scans of ZIF materials (ZIP)

AUTHOR INFORMATION

Corresponding Author

*sankar.nair@chbe.gatech.edu

ORCID

David S. Sholl: 0000-0002-2771-9168

Sankar Nair: 0000-0001-5339-470X

Notes

The authors declare no competing financial interest.

ACKNOWLEDGMENTS

This work was supported by the National Science Foundation (NSF-CBET No. 1264874). We thank Dr. R. Nieuwendaal (NIST) for helpful discussions on NMR spectroscopy, B. Pimentel and Prof. R. Lively (Georgia Tech) for assistance with nitrogen physisorption measurements, Dr. F. Rashidi (Georgia Tech) for assistance with collecting XRD patterns, and M. Zhao and Prof. Y. Xia (Georgia Tech) for assistance with ICP-MS measurements.

REFERENCES

(1) Kuppler, R. J.; Timmons, D. J.; Fang, Q.-R.; Li, J.-R.; Makal, T. A.; Young, M. D.; Yuan, D.; Zhao, D.; Zhuang, W.; Zhou, H.-C. *Coord. Chem. Rev.* **2009**, *253*, 3042.

(2) Pimentel, B. R.; Parulkar, A.; Zhou, E.-k.; Brunelli, N. A.; Lively, R. P. *ChemSusChem* **2014**, *7*, 3202.

(3) Li, J.-R.; Ma, Y.; McCarthy, M. C.; Sculley, J.; Yu, J.; Jeong, H.-K.; Balbuena, P. B.; Zhou, H.-C. *Coord. Chem. Rev.* **2011**, *255*, 1791.

(4) Meek, S. T.; Greathouse, J. A.; Allendorf, M. D. *Adv. Mater.* **2011**, *23*, 249.

(5) Czaja, A. U.; Trukhan, N.; Muller, U. *Chem. Soc. Rev.* **2009**, *38*, 1284.

(6) Farha, O. K.; Hupp, J. T. *Acc. Chem. Res.* **2010**, *43*, 1166.

(7) James, S. L. *Chem. Soc. Rev.* **2003**, *32*, 276.

(8) Stock, N.; Biswas, S. *Chem. Rev.* **2012**, *112*, 933.

(9) Wang, Z.; Cohen, S. M. *Chem. Soc. Rev.* **2009**, *38*, 1315.

(10) Tanabe, K. K.; Cohen, S. M. *Chem. Soc. Rev.* **2011**, *40*, 498.

(11) Cohen, S. M. *Chem. Rev.* **2012**, *112*, 970.

(12) Kim, M.; Cahill, J. F.; Fei, H.; Prather, K. A.; Cohen, S. M. *J. Am. Chem. Soc.* **2012**, *134*, 18082.

(13) Phan, A.; Doonan, C. J.; Uribe-Romo, F. J.; Knobler, C. B.; O'Keeffe, M.; Yaghi, O. M. *Acc. Chem. Res.* **2010**, *43*, 58.

(14) Zhang, C.; Lively, R. P.; Zhang, K.; Johnson, J. R.; Karvan, O.; Koros, W. J. *J. Phys. Chem. Lett.* **2012**, *3*, 2130.

(15) Park, K. S.; Ni, Z.; Cote, A. P.; Choi, J. Y.; Huang, R.; Uribe-Romo, F. J.; Chae, H. K.; O'Keeffe, M.; Yaghi, O. M. *Proc. Natl. Acad. Sci. U. S. A.* **2006**, *103*, 10186.

(16) Thornton, A. W.; Dubbeldam, D.; Liu, M. S.; Ladewig, B. P.; Hill, A. J.; Hill, M. R. *Energy Environ. Sci.* **2012**, *5*, 7637.

(17) Zhang, C.; Koros, W. J. *J. Phys. Chem. Lett.* **2015**, *6*, 3841.

(18) Brown, A. J.; Brunelli, N. A.; Eum, K.; Rashidi, F.; Johnson, J. R.; Koros, W. J.; Jones, C. W.; Nair, S. *Science* **2014**, *345*, 72.

(19) Eum, K.; Rownaghi, A.; Choi, D.; Bhave, R. R.; Jones, C. W.; Nair, S. *Adv. Funct. Mater.* **2016**, *26*, 5011.

(20) Hara, N.; Yoshimune, M.; Negishi, H.; Haraya, K.; Hara, S.; Yamaguchi, T. *J. Membr. Sci.* **2014**, *450*, 215.

(21) Kwon, H. T.; Jeong, H.-K. *J. Am. Chem. Soc.* **2013**, *135*, 10763.

(22) Dong, X.; Lin, Y. S. *Chem. Commun.* **2013**, *49*, 1196.

(23) Thompson, J. A.; Blad, C. R.; Brunelli, N. A.; Lydon, M. E.; Lively, R. P.; Jones, C. W.; Nair, S. *Chem. Mater.* **2012**, *24*, 1930.

(24) Eum, K.; Jayachandrababu, K. C.; Rashidi, F.; Zhang, K.; Leisen, J.; Graham, S.; Lively, R. P.; Chance, R. R.; Sholl, D. S.; Jones, C. W.; Nair, S. *J. Am. Chem. Soc.* **2015**, *137*, 4191.

(25) Rashidi, F.; Blad, C. R.; Jones, C. W.; Nair, S. *AIChE J.* **2016**, *62*, 525.

(26) Liao, Y.-T.; Dutta, S.; Chien, C.-H.; Hu, C.-C.; Shieh, F.-K.; Lin, C.-H.; Wu, K. C.-W. *J. Inorg. Organomet. Polym. Mater.* **2015**, *25*, 251.

(27) Deng, H.; Doonan, C. J.; Furukawa, H.; Ferreira, R. B.; Towne, J.; Knobler, C. B.; Wang, B.; Yaghi, O. M. *Science* **2010**, *327*, 846.

(28) Thompson, J. A.; Vaughn, J. T.; Brunelli, N. A.; Koros, W. J.; Jones, C. W.; Nair, S. *Microporous Mesoporous Mater.* **2014**, *192*, 43.

(29) Reinsch, H.; Waitschat, S.; Stock, N. *Dalton Trans.* **2013**, *42*, 4840.

(30) Karagiaridi, O.; Bury, W.; Mondloch, J. E.; Hupp, J. T.; Farha, O. K. *Angew. Chem., Int. Ed.* **2014**, *53*, 4530.

(31) Karagiaridi, O.; Bury, W.; Sarjeant, A. A.; Stern, C. L.; Farha, O. K.; Hupp, J. T. *Chem. Sci.* **2012**, *3*, 3256.

(32) Li, T.; Kozlowski, M. T.; Doud, E. A.; Blakely, M. N.; Rosi, N. L. *J. Am. Chem. Soc.* **2013**, *135*, 11688.

(33) Ni, Z.; Afeworki, M.; Weston, S. C.; Zengel, J.; Stern, D. L. Linker exchange in zeolitic imidazolate frameworks. US Patent 8,920,541B2, Dec. 30, 2014.

(34) Deria, P.; Mondloch, J. E.; Tylianakis, E.; Ghosh, P.; Bury, W.; Snurr, R. Q.; Hupp, J. T.; Farha, O. K. *J. Am. Chem. Soc.* **2013**, *135*, 16801.

(35) Deria, P.; Bury, W.; Hupp, J. T.; Farha, O. K. *Chem. Commun.* **2014**, *50*, 1965.

(36) Burnett, B. J.; Barron, P. M.; Hu, C.; Choe, W. *J. Am. Chem. Soc.* **2011**, *133*, 9984.

(37) Cravillon, J.; Munzer, S.; Lohmeier, S.-J.; Feldhoff, A.; Huber, K.; Wiebcke, M. *Chem. Mater.* **2009**, *21*, 1410.

(38) Zhang, C.; Gee, J. A.; Sholl, D. S.; Lively, R. P. *J. Phys. Chem. C* **2014**, *118*, 20727.

(39) Jayachandrababu, K. C.; Verploegh, R. J.; Leisen, J.; Nieuwendaal, R. C.; Sholl, D. S.; Nair, S. *J. Am. Chem. Soc.* **2016**, *138*, 7325.

(40) Lee, M.; Goldburg, W. I. *Phys. Rev.* **1965**, *140*, A1261.

(41) Leskes, M.; Madhu, P. K.; Vega, S. *Chem. Phys. Lett.* **2007**, *447*, 370.

(42) Taddei, M.; Tiana, D.; Casati, N.; van Bokhoven, J. A.; Smit, B.; Ranocchiari, M. *Phys. Chem. Chem. Phys.* **2017**, *19*, 1551.

(43) Kong, X.; Deng, H.; Yan, F.; Kim, J.; Swisher, J. A.; Smit, B.; Yaghi, O. M.; Reimer, J. A. *Science* **2013**, *341*, 882.

(44) Krajnc, A.; Kos, T.; Zabukovec Logar, N.; Mali, G. *Angew. Chem., Int. Ed.* **2015**, *54*, 10535.

(45) Kamakoti, P.; Sholl, D. S. *Phys. Rev. B: Condens. Matter Mater. Phys.* **2005**, *71*, 014301.

(46) Clauss, J.; Schmidt-Rohr, K.; Spiess, H. W. *Acta Polym.* **1993**, *44*, 1.

(47) Jia, X.; Wolak, J.; Wang, X.; White, J. L. *Macromolecules* **2003**, *36*, 712.

(48) Nieuwendaal, R. C.; Snyder, C. R.; Kline, R. J.; Lin, E. K.; VanderHart, D. L.; DeLongchamp, D. M. *Chem. Mater.* **2010**, *22*, 2930.

(49) Nieuwendaal, R. C.; Ro, H. W.; Germack, D. S.; Kline, R. J.; Toney, M. F.; Chan, C. K.; Agrawal, A.; Gundlach, D.; VanderHart, D. L.; Delongchamp, D. M. *Adv. Funct. Mater.* **2012**, *22*, 1255.

(50) Song, Y.; Hu, D.; Liu, F.; Chen, S.; Wang, L. *Analyst* **2015**, *140*, 623.

(51) Liu, C.; Yan, B. *Photochem. Photobiol. Sci.* **2015**, *14*, 1644.

(52) Koh, K.; Wong-Foy, A. G.; Matzger, A. J. *Chem. Commun.* **2009**, *41*, 6162.

(53) Tang, J.; Salunkhe, R. R.; Liu, J.; Torad, N. L.; Imura, M.; Furukawa, S.; Yamauchi, Y. *J. Am. Chem. Soc.* **2015**, *137*, 1572.

(54) Morris, W.; Doonan, C. J.; Furukawa, H.; Banerjee, R.; Yaghi, O. M. *J. Am. Chem. Soc.* **2008**, *130*, 12626.

(55) Huang, A.; Dou, W.; Caro, J. *J. Am. Chem. Soc.* **2010**, *132*, 15562.

(56) Brown, A. J.; Johnson, J. R.; Lydon, M. E.; Koros, W. J.; Jones, C. W.; Nair, S. *Angew. Chem.* **2012**, *124*, 10767.

(57) Shieh, F.-K.; Wang, S.-C.; Leo, S.-Y.; Wu, K. C. W. *Chem. - Eur. J.* **2013**, *19*, 11139.

DOI: 10.1021/jacs.7b01660